Contents

2

Linear crystal optics for monochromatic plane waves

The physics of three-wave mixing in anisotropic crystals can be conveniently separated into three topics: how a light wave is changed when it enters or exits the crystal, how a light wave propagates in the crystal, and how three-wave mixing occurs in the crystal. Each of these topics can be considered at different levels of complexity, but each begins with a treatment of monochromatic plane waves. This chapter is devoted to the first two topics, linear propagation of monochromatic plane waves in a crystal, and their behavior on entering or exiting the crystal. Chapters 3 & 4 will explain nonlinear mixing of the monochromatic plane waves. Once the behavior of monochromatic plane waves is thoroughly explored, we will show in subsequent chapters how linear combinations of monochromatic plane waves are used to construct realistic beams and pulses, and how the equations that describe those realistic cases are derived and applied.

As a starting point we rewrite Maxwell's equations specifically for monochromatic plane waves. Following the customary procedure, we write the vectors for the polarization, the electric field, and the displacement in complex notation,

$$\mathbf{P} = \frac{1}{2}\left[\boldsymbol{P}e^{-i(\omega t-\mathbf{k}\cdot\mathbf{r})} + \boldsymbol{P}^{*}e^{i(\omega t-\mathbf{k}\cdot\mathbf{r})}\right], \tag{2.1}$$

$$\mathbf{E} = \frac{1}{2}\left[\boldsymbol{E}e^{-i(\omega t-\mathbf{k}\cdot\mathbf{r})} + \boldsymbol{E}^{*}e^{i(\omega t-\mathbf{k}\cdot\mathbf{r})}\right], \tag{2.2}$$

$$\mathbf{D} = \frac{1}{2}\Big[\boldsymbol{D}e^{-i(\omega t-\mathbf{k}\cdot\mathbf{r})} + \boldsymbol{D}^* e^{i(\omega t-\mathbf{k}\cdot\mathbf{r})}\Big]. \tag{2.3}$$

The actual fields are represented by the real quantities $\mathbf{P}$, $\mathbf{E}$, and $\mathbf{D}$, but for many calculations it is more convenient to use the complex envelope functions $\boldsymbol{D}$, $\boldsymbol{E}$, and $\boldsymbol{P}$. These complex vectors are in general functions of (x, y, z, t). However, for monochromatic plane waves, they are independent of space and time so we omit these arguments in this chapter, and treat the envelope functions as simple complex vectors.

We substitute the expansions of Eqs. (2.1)-(2.3) in the wave equation, Eq. (1.13)

$$\boldsymbol{\nabla}\times\boldsymbol{\nabla}\times\mathbf{E} = -\mu_\circ\frac{\partial^2}{\partial t^2}\mathbf{D} = -\mu_\circ\frac{\partial^2}{\partial t^2}\Big[\epsilon_\circ\mathbf{E}+\mathbf{P}\Big]. \tag{2.4}$$

The operator $\boldsymbol{\nabla}$ becomes $(\pm i\boldsymbol{k})$ when it operates on the exponent $(\pm i\boldsymbol{k}\cdot\boldsymbol{r})$. Similarly the operator $(\partial/\partial t)$ becomes $(\pm i\omega)$ when it operates on the exponent $(\pm i\omega t)$. Making these substitutions in Eq. (2.4) and equating the positive (or negative) frequency components on each side of the equation yields

$$\boldsymbol{k}\times\boldsymbol{k}\times\boldsymbol{E} = -\mu_\circ\omega^2\boldsymbol{D}. \tag{2.5}$$

In deriving this equation we assumed that $\boldsymbol{E}$ and $\boldsymbol{D}$ do not change on propagation, so this is a wave equation for eigenpolarized light. This expression implies that $\boldsymbol{D}$ must be normal to $\boldsymbol{k}$, but $\boldsymbol{D}$ is not necessarily parallel to $\boldsymbol{E}$. However, $\boldsymbol{k}$, $\boldsymbol{D}$, and $\boldsymbol{E}$ must lie in a single plane.

We use a similar procedure to rewrite the Poynting vector equation to find the energy flow for monochromatic plane waves. We start with Eq. (1.16), the general Poynting vector equation,

$$\mathbf{S} = \frac{1}{\mu_\circ}\mathbf{E}\times\mathbf{B} = \mathbf{E}\times\mathbf{H}. \tag{2.6}$$

For monochromatic plane waves the third Maxwell equation, Eq. (1.3), relates $\boldsymbol{H}$ to $\boldsymbol{E}$ for eigenpolarized light in a nonmagnetic material by

$$\boldsymbol{H} = \frac{\boldsymbol{k}\times\boldsymbol{E}}{\mu_\circ\omega}. \tag{2.7}$$

Substituting the expansions for $\mathbf{E}$ and $\mathbf{H}$ in Eq. (2.6), equating equal frequency components, and using Eq. (2.7) plus

$$\epsilon_\circ\mu_\circ c^2 = 1, \tag{2.8}$$

we arrive at

$$\langle\mathbf{S}\rangle = \frac{n\epsilon_\circ c}{2}|\boldsymbol{E}|^2\ \hat{\boldsymbol{e}}\times\hat{\boldsymbol{k}}\times\hat{\boldsymbol{e}}, \tag{2.9}$$

where the angle brackets around **S** indicate a time average over the optical cycle. We only care about the time averaged values, so we will leave the brackets off in the remainder of the book, and **S** will be understood to be the time averaged Poynting vector. The unit vector $\hat{\boldsymbol{e}}$ is parallel to the electric field, and the unit vector $\hat{\boldsymbol{k}}$ is parallel to the propagation vector (normal to the wave fronts). From Eq. (2.9) we see that the flow of optical energy, represented by **S**, is perpendicular to $\boldsymbol{E}$, but not necessarily parallel to $\boldsymbol{k}$. However, **S**, $\boldsymbol{E}$, and $\hat{\boldsymbol{k}}$ must lie in a single plane.

It is a good idea to memorize the two pairings of orthogonal vectors we have just derived, ($\boldsymbol{E}\perp\mathbf{S}$) and ($\boldsymbol{D}\perp\boldsymbol{k}$).

The remainder of this chapter consists of finding solutions to Eq. (2.5) in anisotropic crystals. The solutions will allow us to explore linear propagation in biaxial crystals, and to show how uniaxial and isotropic crystals are special cases of biaxial crystals. I choose this approach because it is not difficult to understand propagation in biaxial crystals, and also because the popular nonlinear crystals of the KTP family (KTP, RTP, KTA, RTA, CTA), plus several borate crystals (LBO, CBO, BiBO, YCOB, GdCOB), and $KNbO_3$ are all biaxial.

Our discussion of light propagation in biaxial crystals will progress from a word-and-diagram geometrical sketch to a more mathematical description based on that geometrical picture, and finally to more abstract mathematical derivations based directly on Maxwell's equations and crystal dielectric tensors.

2.1 A geometrical description

The word picture presented in this section is adapted from Born and Wolf's classic text *Principles of Optics* [1]. We consider only crystals that are nonmagnetic (**M**=0) and nonconductive (**J**=0).

The solution to the wave equation for eigenpolarized light,

$$\boldsymbol{k}\times\boldsymbol{k}\times\boldsymbol{E}=-\mu_\circ\omega^2\boldsymbol{D}, \tag{2.10}$$

can be broken into two steps. The first step is to relate $\boldsymbol{D}$ to $\boldsymbol{E}$ in a general way. The second step is to find the particular paired values of $\boldsymbol{D}$ and $\boldsymbol{E}$ that solve the wave equation.

2.1.1 Relating $\boldsymbol{D}$ to $\boldsymbol{E}$

Any two vector quantities in a nonisotropic crystal are generally related by a (3×3) tensor. In our case of $\boldsymbol{D}$ and $\boldsymbol{E}$, the relation is

$$\boldsymbol{D}=\boldsymbol{\epsilon}\cdot\boldsymbol{E}, \tag{2.11}$$

where $\boldsymbol{\epsilon}$ is the symmetric (3×3) dielectric tensor. It will be more convenient to use this equation in the form

$$\boldsymbol{E} = \boldsymbol{\epsilon}^{-1}\cdot\boldsymbol{D}. \tag{2.12}$$

As we discuss in Chapter 13, Eq. (2.12) can be associated with a three dimensional ellipsoid with principal axes n_x, n_y, and n_z defined by

$$n_x = \sqrt{\epsilon_{xx}/\epsilon_\circ}\,, \tag{2.13}$$

$$n_y = \sqrt{\epsilon_{yy}/\epsilon_\circ}\,, \tag{2.14}$$

$$n_z = \sqrt{\epsilon_{zz}/\epsilon_\circ}\,. \tag{2.15}$$

This ellipsoid has various names in the literature. We will call it the D-ellipsoid because, as we will see, it relates a given $\boldsymbol{D}$ to its paired $\boldsymbol{E}$. The D-ellipsoid is diagrammed in Fig. 2.1 where, for the purpose of illustration, the ellipticity is greatly exaggerated. In practice the lengths of the principal axes usually differ by 5% or less.

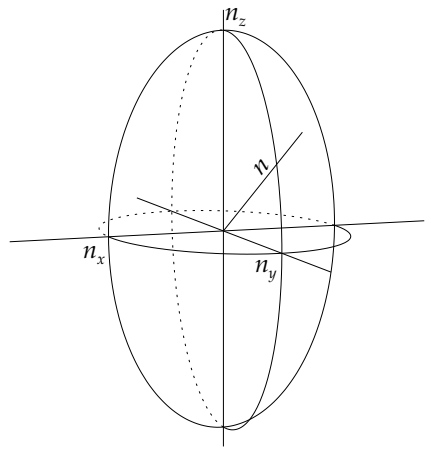

FIGURE 2.1. D-ellipsoid shown with the principal optical frame $\{x, y, z\}$ which is aligned to the primary axes of the ellipsoid with the convention $(n_x < n_y < n_z)$.

For biaxial crystals the three principal axes have different lengths, and we adopt the standard labeling with $(n_x < n_y < n_z)$. For uniaxial crystals two of the axes have equal length, while for isotropic crystals all three axes have equal length. These are limiting cases of the biaxial crystal, so an understanding of biaxial crystals will be easy to apply to them. We will

relate the orientation of the D-ellipsoid to the underlying crystal structure in Chapter 15. For now it is sufficient to know the D-ellipsoid exists for any crystal.

The D-ellipsoid represents the dielectric response for all orientations of $\boldsymbol{D}$. If $\boldsymbol{D}$-extended is drawn as a vector from the origin through the ellipsoid surface, the electric field $\boldsymbol{E}$ associated with $\boldsymbol{D}$ is parallel to the surface normal of the ellipsoid at the point where $\boldsymbol{D}$ intersects the surface. In general $\boldsymbol{E}$ is not quite parallel to $\boldsymbol{D}$. The two are exactly parallel only when they are aligned with one of the principal axes of the D-ellipsoid.

2.1.2 Finding the eigenpolarizations

As we showed earlier, the relation ($\boldsymbol{D} \perp \boldsymbol{k}$) must hold in order to satisfy the wave equation. If we consider a wave propagating along direction $\hat{\boldsymbol{k}}$, as shown in Fig. 2.2, $\boldsymbol{D}$ must lie in the plane normal to $\hat{\boldsymbol{k}}$. This plane passes through the center of the D-ellipsoid and intersects the ellipsoid in an ellipse that we can call the n-ellipse. The $\boldsymbol{E}$ field associated with $\boldsymbol{D}$ must be aligned normal the D-ellipsoid and thus normal to the n-ellipse. However, $\boldsymbol{E}$ does not generally lie in the plane of the n-ellipse.

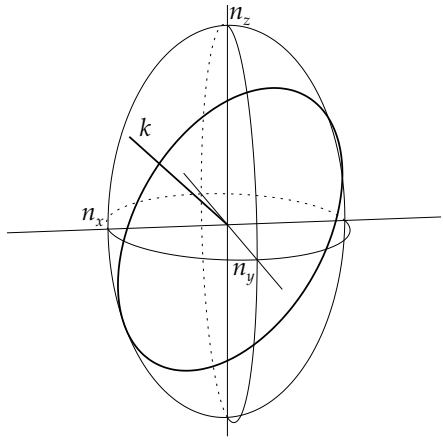

FIGURE 2.2. D-ellipsoid and propagation vector, $\boldsymbol{k}$. The plane normal to $\boldsymbol{k}$ that passes through the origin intersects the D-ellipsoid in the n-ellipse indicated by the heavy line. The eigenpolarization planes coincide with the major and minor axes of this n-ellipse, and the associated refractive indices are equal to the semi major and semi minor axes of the ellipse.

In order to satisfy the wave equation, $\boldsymbol{E}$ must lie in the same plane as $\boldsymbol{k}$ and $\boldsymbol{D}$. Otherwise the vector quantities on the two sides of Eq. (2.10)

would not be parallel. This condition can be met only if $\boldsymbol{D}$ lies along one of the principal axes of the n-ellipse. There are two possible solutions to the wave equation corresponding to $\boldsymbol{D}$ lying along either of the principal axes of the n-ellipse. The $\boldsymbol{D}$ vectors of the two solutions are thus orthogonal to one another, and in combination with $\boldsymbol{k}$ define two eigenpolarization planes that contain $\boldsymbol{k}$ and the paired solutions for $\boldsymbol{D}$ and $\boldsymbol{E}$. Only waves with $\boldsymbol{D}$ aligned along the major or minor axis of the n-ellipse propagate without changes to the direction of $\boldsymbol{D}$ or $\boldsymbol{E}$, that is as eigenpolarizations. The corresponding two refractive index values correspond to the lengths of the two principal axes of the n-ellipse. We use *hi* or *lo* to label the eigenpolarization associated with the higher or lower refractive index.

To summarize, the problem of finding the eigenpolarizations and their refractive indices is reduced to the problem of constructing the D-ellipsoid based on the crystal's dielectric tensor, followed by defining a propagation vector $\boldsymbol{k}$. The n-ellipse is then defined in the plane normal to $\boldsymbol{k}$, and the two eigenpolarization planes are those defined by $\boldsymbol{k}$ and the major and minor axes of the n-ellipse. The two corresponding refractive indices are given by the lengths of the semi major and semi minor axes of the n-ellipse.

2.1.3 Optical axes of biaxial crystals

Suppose we start with the propagation vector parallel to the z axis of the D-ellipsoid and continuously rotate it in the xz plane until it is parallel to x. Initially, when the propagation is along z, the n-ellipse lies in the xy plane, and n_{hi}, the higher index, must be equal to n_y, and n_{lo} must be equal to n_x. As the propagation direction rotates away from z toward the x, the n-ellipse pivots about the y-axis. Thus the y direction remains an eigenpolarization with the refractive index n_y, but the second refractive index increases as the angle increases, going from n_x for propagation along z to n_z for propagation along x. The second index starts out smaller than n_y and finishes larger than n_y, so at some intermediate angle it must be equal to n_y. At that angle the n-ellipse must be a circle with both refractive indices equal to n_y. This propagation direction is known as the optic axis, and its angle relative to z is traditionally labeled Ω. By symmetry there must be a second equivalent optic axis on the opposite side of the z-axis at $(-\Omega)$. As the propagation angle sweeps through Ω the major and minor axes of the n-ellipse swap places. For angles smaller than Ω the major axis is parallel to y, while for angles larger than Ω the minor axis is parallel to y.

2.1.4 Propagation outside the principal planes

When the k-vector lies outside the three principal planes, xy, xz, or yz, the n-ellipse and its eigenpolarization directions are generally rotated so the eigenpolarizations do not align with the axes of the D-ellipsoid. Figure 2.3 illustrates the two eigenpolarization directions for various propagation direction lying in one octant for the biaxial crystal $KNbO_3$. The eigenpolarizations twist as the propagation direction changes, but they are always orthogonal to one another. The other octants are images of this one reflected in the three principal planes, xy, yz, and xz. The angle of the optical axis, Ω, uniquely determines the entire eigenpolarization map for a crystal. All crystals with identical optical axis directions share the same eigenpolarization map.

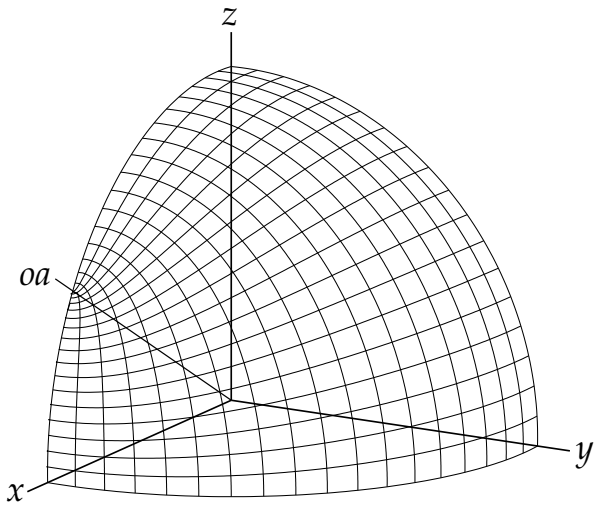

FIGURE 2.3. Eigenpolarization pairs plotted against the propagation direction in one octant of the biaxial crystal $KNbO_3$. The polarization directions for the *lo* refractive index follow lines originating on the yz arc, while the polarization directions for the *hi* refractive index follow lines originating on the xy arc. The optic axis is labeled *oa*. The other octants are reflections of this one in the three principal planes, xy, yz, or xz.

2.1.5 Poynting vector walk off

As described earlier, the electric field $\boldsymbol{E}$ paired with $\boldsymbol{D}$ is normal to the surface of the D-ellipsoid at the point where $\boldsymbol{D}$ intersects it, so $\boldsymbol{E}$ is not in general parallel to $\boldsymbol{D}$. For an eigenpolarization the point of intersection coincides with either the major or the minor axis of the n-ellipse, so the tilt of $\boldsymbol{E}$ must lie in the plane containing both $\boldsymbol{D}$ and $\boldsymbol{k}$. The small angle between $\boldsymbol{D}$ and $\boldsymbol{E}$ is conventionally labeled ρ. $\boldsymbol{E}$ is tilted relative to $\boldsymbol{D}$ in the direction of diminishing refractive index.

Recall that $\boldsymbol{E}$ and $\mathbf{S}$ are orthogonal. This implies that the angle between $\boldsymbol{k}$ and $\mathbf{S}$ is also ρ. Each of the eigenpolarizations has an associated Poynting vector walk off angle that we label ρ_{hi} or ρ_{lo}. These tilts are illustrated in Fig. 2.4.

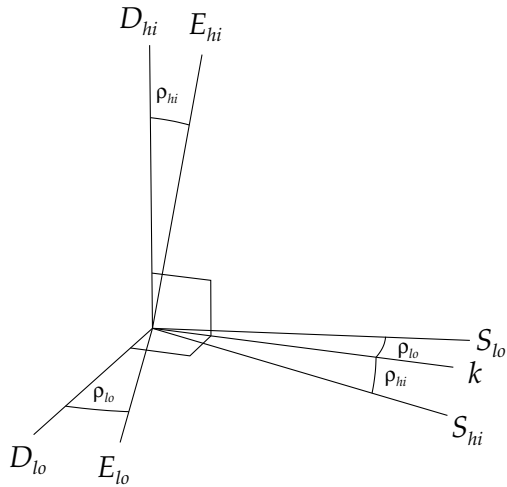

FIGURE 2.4. Vectors $\boldsymbol{D}_{hi}$, $\boldsymbol{E}_{hi}$, $\mathbf{S}_{hi}$, and $\boldsymbol{k}$ lie in a single plane while vectors $\boldsymbol{D}_{lo}$, $\boldsymbol{E}_{lo}$, $\mathbf{S}_{lo}$, and $\boldsymbol{k}$ lie in an orthogonal plane. Walk off angle ρ_{hi} is the angle between $\boldsymbol{D}_{hi}$ and $\boldsymbol{E}_{hi}$ and also the angle between $\boldsymbol{k}$ and $\mathbf{S}_{hi}$. Walk off angle ρ_{lo} is the angle between $\boldsymbol{D}_{lo}$ and $\boldsymbol{E}_{lo}$ and also the angle between $\boldsymbol{k}$ and $\mathbf{S}_{lo}$.

Because walk off occurs in the eigenpolarization planes, the lines in Fig. 2.3 that show the eigenpolarization directions also indicate the directions of the two Poynting vector walk off angles. For the *hi* eigenpolarization (curves originating on the xy arc), the energy flow is tilted along the *hi* eigenpolarization direction in the direction away from the xy plane, while for the *lo*-index polarization (curves originating on the yz plane) the

energy flow is tilted along the *lo* eigenpolarization direction toward the *yz* plane.

Walk off always tilts **S** toward the direction of lower refractive index, so if $\boldsymbol{k}$ is pivoted slightly in the plane of the *lo* eigenpolarization in the direction of walk off, n_{lo} decreases but n_{hi} is unaltered. This means that the lines in Fig. 2.3 that indicate the directions of the *lo* eigenpolarization (curves originating on the *yz* plane) are also curves of constant n_{hi}. Similarly, the *hi* eigenpolarization directions (curves originating on the *xy* plane) are curves of constant n_{lo}. For example, for propagation directions lying in the *yz* plane, the *hi* eigenpolarization lies in the *yz* plane and n_{hi} varies with angle, but the *lo* eigenpolarization is normal to the *yz* plane and $n_{lo} = n_x$, independent of angle. Similarly, along each of the lines originating on the *xy* arc, n_{lo} is constant, with a different value for each line, varying from n_x for the line lying in the *yz* plane to n_y for the line lying in the *xz* plane and terminating at the optic axis.

For propagation in a principal plane one of the walk off angles becomes zero. For example, propagation in the *yz* plane makes ($\rho_{lo} = 0$), while propagation in the *xy* plane makes ($\rho_{hi} = 0$). Propagation in the *xz* plane makes ($\rho_{lo} = 0$) for directions between *oa* and *x*, and ($\rho_{hi} = 0$) for directions between *oa* and *z*.

2.1.6 Hi and lo index surfaces

We have explained that there are two refractive indices associated with each propagation direction. They can be represented by double surfaces as shown in Fig. 2.5. The distance from the origin to the outer surface along any propagation direction is n_{hi}. The distance to the inner surface is n_{lo}. The two surfaces touch only at their point of intersection with the optic axes. The Poynting vector for a beam with *lo* polarization is normal to the inner surface, the Poynting vector for the beam with *hi* polarization is normal to the outer surface. The corresponding $\boldsymbol{E}$ fields are tangent to the surfaces.

2.1.7 Uniaxial crystals

The symmetry of the crystal structure for certain classes of crystals requires that two of the principal refractive indices be exactly equal (see Chapter 15). In the transition from biaxial to uniaxial there are two possibilities: the intermediate index n_y can approach the high index ($n_y \rightarrow n_z$) or the low index ($n_y \rightarrow n_x$). If ($n_y \rightarrow n_z$), the two optic axes tilt toward the *x* axis, while if ($n_y \rightarrow n_x$), the optic axes tilt toward the *z* axis. The left diagram in Fig. 2.6 shows the eigenpolarization directions for the crystal DLAP which has principal indices at 1064 nm of ($n_x = 1.496$), ($n_y = 1.558$),

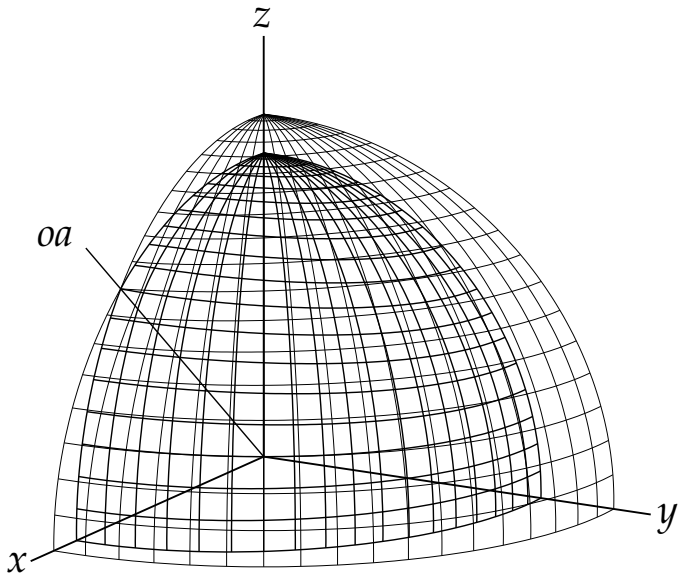

FIGURE 2.5. The two n surfaces. The distance from the origin to the outer surface at each value of (θ, ϕ) is $n_{hi}(\theta, \phi)$, while the distance to the inner surface is $n_{lo}(\theta, \phi)$. The **E** field for an eigenpolarization is tangent to the corresponding surface, and its Poynting vector **S** is normal to the corresponding surface. The optic axis *oa* is the only point where the two surfaces touch.

and $(n_z = 1.565)$. Its optic axis lies near the x axis. The right diagram in Fig. 2.6 shows the eigenpolarization directions for the crystal KTA which has principal indices at 1064 nm of $(n_x = 1.782)$, $(n_y = 1.787)$, and $(n_z = 1.868)$. Its optic axis lies near the z axis.

If n_y becomes exactly equal to n_x the two optic axes merge into a single optic axis oriented along z. The eigenpolarization directions then lie along the latitude and longitude lines as shown in Fig. 2.7. The *hi*-index wave, polarized along a line of constant longitude, is called the extraordinary, or *e*-wave, while the *lo*-index wave, polarized along a line of constant latitude, is called the ordinary, or *o*-wave. The n_o surface is spherical with radius $n_x(= n_y)$, while the n_e surface is an oblate ellipsoid of revolution with polar radius of $n_x(= n_y)$ and equatorial radius n_z. The left hand diagram

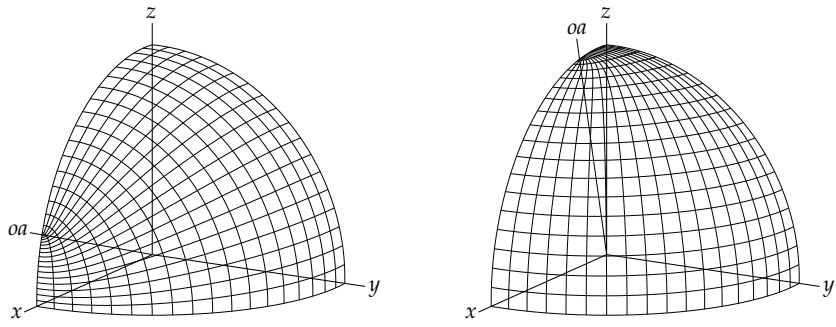

FIGURE 2.6. Eigenpolarization and walk off directions for DLAP (left) and KTA (right). The line labeled *oa* is the optic axis. The other octants are reflections of this one in the three principal planes.

of Fig. 2.8 shows a slice through the double n-surface for such a positive uniaxial crystal. The o-wave has no Poynting vector walk off, while the walk off of the e-wave is toward the z axis.

On the other hand, if n_y becomes exactly equal to n_z, the crystal is negative uniaxial and the two optic axes converge to a single axis lying along x. The eigenpolarization contours converge on the x axis rather than the z axis. However, for such crystals it is customary to abandon the convention $(n_x < n_y < n_z)$ and relabel the unique axis from x to z. The eigenpolarization directions then are identical to those shown in Fig. 2.7. The ordinary or n_o surface is again spherical while the extraordinary or n_e surface is a prolate ellipsoid of revolution. A cross section through the double index surfaces for a negative uniaxial crystal shown on the right in Fig. 2.8. Poynting vector walk off of the e-wave is away from the z axis for a negative uniaxial crystal.

2.1.8 Isotropic crystals

If $(n_x = n_y = n_z)$, all three refractive indices are equal so the D-ellipsoid is a sphere. The crystal is isotropic, meaning all propagation directions and polarizations are equivalent. There are no unique eigenpolarization directions determined by the crystal's dielectric response, so all polarizations are eigenpolarizations.

Exercise 1 illustrates computation of the *hi* and *lo* refractive indices plus the walk off angles, for any propagation direction in a biaxial or uniaxial crystal using the SNLO function RefInd.

9

Mixing CW monochromatic beams in optical cavities

Nonlinear mixing inside an optical cavity provides several benefits. Foremost, the cavity enhances the strength of the optical fields and thus the strength of mixing, permitting efficient mixing with beams of only a few mW or even μW. The cavity also helps improve the beam quality of the resonated waves by acting as a spatial mode filter. The tradeoff is that it is necessary to match the input light to both the longitudinal and transverse modes of the cavity. This is not always easy in the laboratory. Three different wavelengths must sometimes be resonant with the same cavity and still satisfy ($\omega_1 + \omega_2 = \omega_3$). Simply changing the cavity length cannot accommodate all three waves so additional dispersive tuning mechanisms must be used. Similarly, if the quality of the input beams is not outstanding, much of their power will not match the transverse mode and cannot be used. Of course, in theory and in models it is trivial to meet the ideal conditions, and we will routinely assume perfect cavity matching. We will consider only monochromatic beams tuned to cavity resonance, either in the plane-wave limit or with real diffracting beams. All of our analytical treatments will be based on plane waves, but we will show in the modeling exercises at the end of the chapter that there is usually a close correspondence with focused Gaussian beams.

Analysis of cavity nonlinear mixing is really a study in the management of parasitic cavity losses. In the absence of such loss, and in the plane-wave limit, parametric oscillators and sum or difference frequency mixers could always be designed for high efficiency. The cavity enhancements could be

made as high as necessary for efficient mixing even with weak beams. In real devices cavity losses limit the enhancement, and set a lower limit on the input powers required for high efficiency. We will characterize parasitic cavity loss by parameter V, which we typically add to the actual transmission of one of the cavity mirrors. The strength of each resonated wave circulating inside the cavity is limited to a maximum value of approximately (S/V) where S is the irradiance of the input wave or the emitted wave.

In a plane-wave treatment, each three-wave-mixing process has a characteristic irradiance defined by

$$S_\circ = \frac{\epsilon_\circ c^3 n_1 n_2 n_3}{2 d_{\text{eff}}^2 \omega_1 \omega_2 L^2}. \tag{9.1}$$

Without cavity enhancement, strong mixing requires the irradiance at least one of the input waves to be comparable to $S_\circ$. A cavity that resonates one or more of the waves permits strong mixing with weaker input beams. For example, resonating one of the waves with a round trip loss of V_a requires a minimum input irradiance of approximately $(S_\circ/V_a)$. Resonating a second wave with loss V_b further reduces the required input irradiance to $(S_\circ/V_aV_b)$, while resonating a third wave with loss V_c requires an irradiance comparable to $(S_\circ/V_aV_bV_c)$.

The variety of possible cavity mixers is large, and we will try to take at least a cursory look at each. However, first we will develop some common themes so we can simplify the individual analyses. The first is how to design a resonant cavity. Possibilities abound here as well, but because ring cavities are practical and are the easiest to analyze, we will concentrate on bow tie ring cavities that use two identical curved mirrors bracketing the crystal with two auxiliary mirrors to complete the cavity. Much of our discussion and modeling can be translated to linear cavities or to asymmetric ring cavities, but we won't deny you the thrill of analyzing these on your own. A second theme is impedance matching. This involves adjusting mirror reflectivities so an input beam is totally absorbed by the cavity, with no reflection at the input mirror. This maximizes conversion efficiency for the impedance matched wave. We also consider the emission efficiency for waves that are created inside the cavity. Another theme is the time reversal symmetry between an ideal sum frequency mixer and an ideal optical parametric oscillator. This symmetry is broken by cavity losses, but the equivalence is illuminating when considering the stability of sum frequency mixers. We will give a general description of these themes and then we will analyze individual designs in detail. Our discussions are organized by application, starting with the design of optical cavities, followed by discussion of intracavity sum frequency mixers, followed by optical parametric oscillators, and finishing with difference frequency mixers.

There is no essential difference between numerical models of cavity sum- or difference-frequency mixing or optical parametric oscillation. In a nu-

merical model it is a simple matter to adjust the mirror reflectivities and input beam powers to accommodate any CW cavity mixing process whether singly-, doubly-, or triply-resonant. Transverse beam effects due to walk off or noncollinear beams can also be handled by numerical models, but we will not consider them here.

SNLO functions PW-cav-LP and 2D-cav-LP are appropriate for CW monochromatic intracavity mixing of all varieties. We will use a standard set of inputs for most of the examples in this chapter, changing only the input powers and the input and output mirror reflectivities to accommodate different devices. This is intended to facilitate easy comparisons among designs.

9.1 Cavity design and mixing analysis

Because CW beams are usually limited in power, efficient mixing generally requires the use of a resonant cavity to enhance the power at the nonlinear crystal. Stable cavities also focus the circulating beams in the nonlinear crystal. A wide variety of cavities have been used but two are particularly popular, the symmetric linear cavity, and the symmetric bow tie ring cavity. They are diagrammed in Fig. 9.1. The advantages of the linear cavity are compactness and simplicity. Its disadvantages are that it can be difficult to achieve a desired reflectivity of all three waves using only two mirrors; in particular it can be difficult to achieve low levels for the waves that are not supposed to be resonated. Reflection back into the lasers may also be a problem with a linear cavity. The standing waves of a linear cavity can also pose problems, not because of spatial hole burning as occurs in lasers, but because of the potential for optical damage caused by the enhanced field strengths at the anti nodes, and because of possible inconsistent frequency tuning depending on whether nodes or anti nodes align with slightly lossy intra cavity surfaces. It can also be difficult to control the relative phases of the reflected waves, an important consideration if all three waves are reflected. Many of these difficulties can be overcome by using the ring cavity, but at the cost of a longer cavity with narrower resonances, higher expenses with two additional mirrors, and more real estate.

9.1.1 Stable cavity design

Ring cavity

We first consider an empty or monolithic ring cavity. We will consider linear cavities and cavities containing a crystal later. The popular symmetric bow tie ring cavity is shown in Fig. 9.1. An equivalent three-mirror cavity

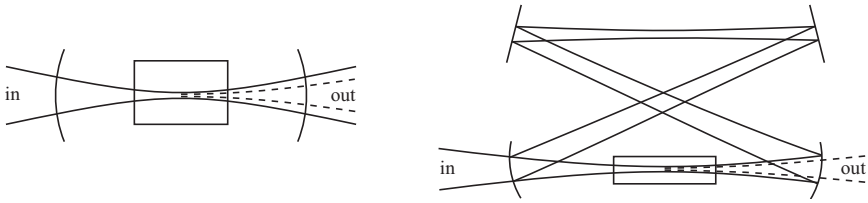

FIGURE 9.1. Examples of stable cavities. A symmetric standing wave cavity is shown on the left; a folded ring cavity is shown on the right.

replaces the two plane mirrors with a single plane mirror located at the crossing point of the beams to direct the beam from one curved mirror to the other. Either version uses two curved mirrors of curvature R and contains two beam waists, one located midway between the curved mirrors in leg (L_1), the other located midway on the longer leg (L_2). The crystal is usually centered at the midpoint of L_1 as diagrammed in Fig. 9.1.

The first cavity requirement is that the radii of curvature of the resonated beam at the curved mirrors satisfy

$$\frac{1}{R_{c1}} + \frac{1}{R_{c2}} = \frac{2}{R_m}, \tag{9.2}$$

where R_{c1} and R_{c2} are the wavefront curvatures for the beams in the two legs at the curved mirrors, and R_m is the radius of curvature of the curved mirrors. The second cavity requirement is that the beam sizes for the two legs must be equal at each curved mirror. Using these two conditions plus the usual expressions for Gaussian beam size w and phase curvature R yields the following condition on the Rayleigh ranges for the foci in the two legs of the cavity

$$z_{R1} = \frac{1}{2}\left[\frac{L_1 R_m^2 + L_2 R_m^2 - 2L_1 L_2 R_m - L_1^2 R_m + L_1^2 L_2}{R_m - L_2}\right]^{1/2}, \tag{9.3}$$

$$z_{R2} = \frac{1}{2}\left[\frac{L_1 R_m^2 + L_2 R_m^2 - 2L_1 L_2 R_m - L_2^2 R_m + L_1 L_2^2}{R_m - L_1}\right]^{1/2}. \tag{9.4}$$

For the empty cavity we can select R_m and vary L_1 and L_2 keeping the ratio ($q = L_2/L_1 > 1$) fixed. There are two stability zones, the first with ($0 < L_1 < R_m/q$) places the smaller waist in the longer leg L_2, and the second with ($R_m < L_1 < R_m[1 + 1/q]$) places the smaller waist in the shorter leg L_1. Outside these zones a Gaussian beam cannot be resonated. The second zone is used in most cases because it provides a tighter focus in a crystal positioned between the curved mirrors. The normalized Rayleigh range in this stability zone, derived from Eq. (9.3), can be written in terms

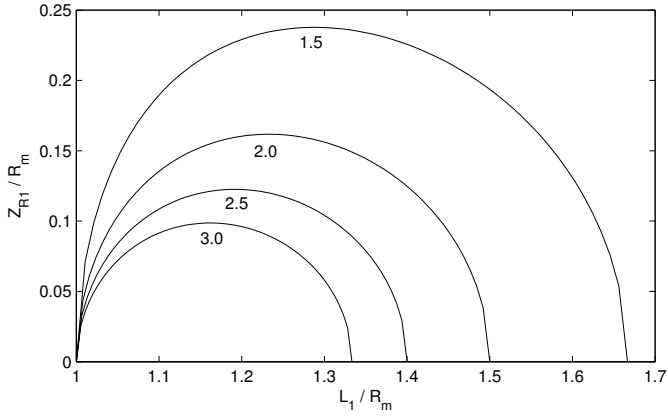

FIGURE 9.2. Empty cavity Rayleigh range z_{R1} normalized to the mirror radius of curvature R_m versus (L_1/R_m) for four values of the ratio of leg lengths $(L_2/L_1 = q = \{1.5, 2.0, 2.5, 3.0\})$.

of L_1 and q as

$$\frac{z_{R1}}{R_m} = \left[\frac{(L_1/R_m)(1 - L_1/R_m)(1 + q - qL_1/R_m)}{4(1 - qL_1/R_m)}\right]^{1/2}. \tag{9.5}$$

Figure 9.2 shows (z_{R1}/R_m) plotted versus (L_1/R_m) for $(q = \{1.5, 2.0, 2.5, 3.0\})$. Increasing the length of the second leg L_2 increases q and gives a tighter focus in leg L_1 and a smaller stability range for L_1.

Usually the best operating point is near the middle of the stability range where $w_{\circ 1}$ and z_{R1} are nearly maximized. The mid point of the stability range is at

$$\frac{L_1}{R_m} = \left[1 + \frac{1}{2q}\right], \tag{9.6}$$

where the normalized Rayleigh range is

$$\frac{z_{R1}}{R_m} = \frac{1}{4q}\left[\frac{2q+1}{2q-1}\right]^{1/2}. \tag{9.7}$$

Linear cavity

The linear cavity is a special case of the ring cavity with $(q = 1)$ $(L_1 = L_2 = L)$. Equation (9.3) becomes

$$z_R = \frac{1}{2}\left[L\,(2R_m - L)\right]^{1/2}, \tag{9.8}$$

and solving this equations for L gives

$$L = R_m \pm \sqrt{R_m^2 - 4z_R^2}\,. \tag{9.9}$$

The two stability zones merge into one with a stability range ($0 < L < 2R_m$). The plot of (z_R/R_m) *vs.* ($L/2R_m$), corresponding to Fig. 9.2, is a semicircle of radius (1/2) centered at ($L/2R_m = 1/2$).

When ($L \ll R_m$) the cavity is nearly planar, the Rayleigh range is much longer than the cavity, and the round trip Gouy phase is nearly zero. When L approaches its maximum stable length of ($2R_m$) the cavity is nearly concentric, the waist is small, the Rayleigh range is much shorter than the cavity, and the round trip Gouy phase approaches 2π. At the mid point of the stability zone where ($L = R_m$), the cavity is confocal, the Rayleigh range has its maximum value of ($z_R = L/2$), and the round trip Gouy phase is π. The beam size at the waist is ($w_\circ = \sqrt{R_m/k}$), and the beam size at the mirrors is ($w = \sqrt{2}w_\circ$). The confocal cavity offers the least sensitivity to mirror misalignment among symmetric linear cavities.

In a confocal cavity the axial modes associated with the symmetric transverse modes all have the same resonance frequency. This means that any symmetric monochromatic input beam can be resonated without losses caused by transverse mode filtering. This contrasts with a non-confocal cavity in which the different transverse modes have differing resonant frequencies, so the cavity can act as a mode filter, resonating one transverse mode at a time. If you wish to use the cavity to help maintain good mode quality, the confocal cavity is not the best choice. However, if you wish to resonate the highest power for an imperfect beam it is. A ring cavity is always similar to the nonconfocal configurations of the linear cavity, with nondegenerate resonant frequencies.

Designing a resonant cavity

The first choice is whether to use a ring or linear cavity. A ring is often chosen to minimize feedback to a laser. A linear cavity is often chosen for compactness. If non-Gaussian beams are to be resonated a confocal linear cavity can be used. The equations above were derived for monolithic cavities where the medium filling the cavity can be a crystal or air. If the cavity contains a crystal that does not fill the cavity, it is necessary to slightly modify the design, as explained next.

If a ring is chosen, one approach is to first choose the ratio ($q = L_2/L_1$), perhaps based on space requirements for optical mounts or perhaps based on the desired focal waist size. Often a value of the Rayleigh range in the crystal z_{Rc} is targeted, usually based on the crystal length and consideration of the mixing strength. The Rayleigh range in air is then ($z_{R1} = z_{Rc}/n$) where n is the crystal refractive index. Using z_{R1} in Eqs. (9.7) and (9.6) we

can find values for R_m and L_1. We then add the crystal to the ring cavity by lengthening L_1 to L_1' where

$$L_1' = L_1 + L_{\text{crystal}}\big(1 - 1/n\big), \tag{9.10}$$

and if L_2 is unchanged, the beam waist, the round trip Gouy phase, and the beam size at the mirrors do not change.

To add a crystal to a linear cavity the same change in cavity length is used, again with no change to the waist size or the Gouy phase.

Mode matching

Once a suitable cavity is built it is desirable to mode match each resonated input beam to a cavity mode, meaning its size and curvature at the input mirror must match the size and curvature of the fundamental cavity mode at that location. The cavity length must also be adjusted so its axial mode coincides with the wavelength of the input beam. If the beam quality is imperfect, meaning it contains higher order transverse modes, only the lowest order Gaussian content of the beam will fully resonate, unless the cavity is confocal.

SNLO function 2D-cav-LP can model asymmetric linear and ring cavities but here we will use only symmetric cavities, and the SNLO function Cavity can be used to design them. Exercise 1 illustrates how to design a stable linear cavity using the Cavity function. Exercise 2 illustrates resonating light in a stable linear cavity using 2D-cav-LP. Exercise 3 illustrates mode filtering in a stable linear cavity using 2D-cav-LP. Exercise 4 illustrates one way to design a stable ring cavity using Cavity. Exercise 5 illustrates resonating light in a stable ring cavity using 2D-cav-LP.

9.1.2 Impedance matching

The purpose of a resonant cavity is usually to enhance the strengths of the fields to improve mixing efficiency. This is best achieved by impedance matching the beam to the cavity. Impedance matching is a term borrowed from radio frequency technology where it usually means that the reflected power from a broadcast antenna or tuned filter is minimized. In optics it means the light reflected from the input mirror of the optical cavity is minimized by adjusting the reflectivities of the cavity mirrors. Referring to Fig. 9.3, impedance matching means the field E^{ref} reflected from the

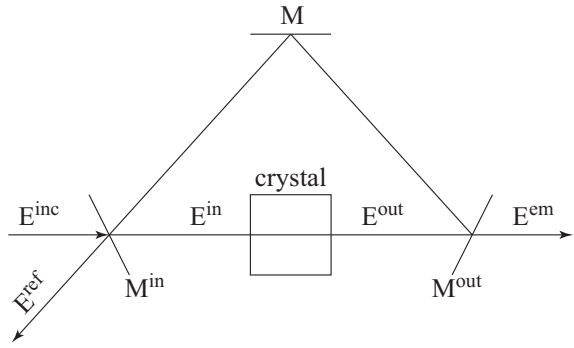

FIGURE 9.3. Reference diagram for ring build up cavity for sum frequency mixing calculations. The red waves enter mirror M^{in} and the blue wave exits mirror M^{out}. Mirror M reflects all wavelengths.

cavity input mirror is nulled. The field equations at the input mirror of our reference cavity are

$$E^{ref} = -E^{inc} r^{in} + E^{out} r^{out} t^{in}, \tag{9.11}$$

$$E^{in} = E^{inc} t^{in} + E^{out} r^{out} r^{in}, \tag{9.12}$$

where the field reflection and transmission coefficients t and r are real valued, and the irradiance coefficients T and R are the squares of the field coefficients t and r. We assume the cavity is tuned to resonate the wave so all of the fields can be treated as real valued as well. Setting $(E^{ref} = 0)$ in Eq. (9.11) gives

$$E^{inc} = E^{out} \frac{r^{out} t^{in}}{r^{in}}. \tag{9.13}$$

Substituting this in Eq. (9.12) and using $(t^2 + r^2 = 1)$ gives the impedance matching condition

$$E^{in} = \frac{E^{inc}}{t^{in}}. \tag{9.14}$$

In the analyses to come, it will be handy to use the irradiance version of this relation

$$S^{in} = \frac{S^{inc}}{T^{in}}, \tag{9.15}$$

where S is defined

$$S = \frac{\epsilon_\circ c n}{2} |E|^2. \tag{9.16}$$

Substituting Eq. (9.14) in Eq. (9.12) leads to the impedance matching relation

$$r^{in} = t^c r^{out}, \tag{9.17}$$

where t^c is the crystal transmission defined by

$$t^c = \frac{E^{out}}{E^{in}}. \tag{9.18}$$

The crystal transmission can be greater or less than one depending on whether the wave of interest experiences net gain or loss in the crystal.

We can show that impedance matching is equivalent to maximizing the value of E^{in} which maximizes the mixing strength. Using Eq. (9.18), Eq. (9.12) can be rearranged to

$$\frac{E^{in}}{E^{inc}} = \frac{t^{in}}{1 - t^c r^{out} r^{in}} = \frac{\sqrt{1 - r^{in} r^{in}}}{1 - t^c r^{out} r^{in}}. \tag{9.19}$$

It is straightforward to differentiate the right hand side of this expression with respect to r^{in} to show the ratio (E^{in}/E^{inc}) is maximized when the impedance matching condition of Eq. (9.17) is satisfied. Of course, in nonlinear devices the value of t^c depends on the strengths of all three optical fields, so calculating the impedance matching condition requires careful analysis that included the nonlinear mixing process.

Equation (9.17) expresses the familiar idea that impedance matching requires the input mirror reflectivity to equal the feedback from the remainder of the cavity. For later reference it will be handy to know the irradiance change ΔS in the crystal implied by impedance matching. This is calculated from Eqs. (9.13) and (9.14) as

$$\Delta S = S^{out} - S^{in} = \left(|E^{out}|^2 - |E^{in}|^2\right)\frac{\epsilon_\circ c}{2}, \tag{9.20}$$

$$\Delta S = \left(\frac{R^{in}}{T^{in} R^{out}} - \frac{1}{T^{in}}\right)|E^{inc}|^2 \frac{\epsilon_\circ c}{2}, \tag{9.21}$$

$$\Delta S = S^{inc} \frac{R^{in} - R^{out}}{T^{in} R^{out}}. \tag{9.22}$$

Also for later reference, other handy relations that hold for an impedance matched wave include:

$$\Delta S = S^{em} \frac{R^{in} - R^{out}}{T^{out} R^{in}}, \tag{9.23}$$

$$\Delta S = S^{in} \frac{R^{in} - R^{out}}{R^{out}}, \tag{9.24}$$

$$\Delta S = S^{out} \frac{R^{in} - R^{out}}{R^{in}}. \tag{9.25}$$

It is frequently necessary to search for the impedance matching conditions using numerical models. It that search it is useful to have a signature that

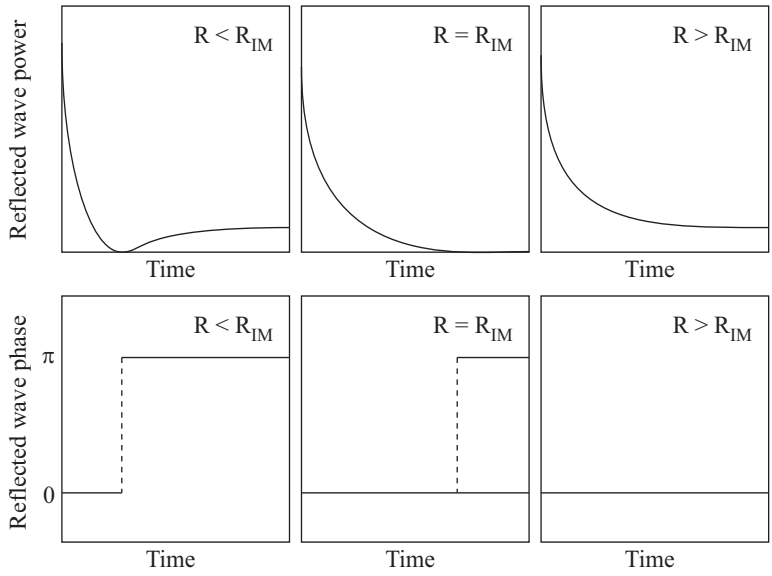

FIGURE 9.4. Time evolution of the power and phase of the reflected wave at the input mirror of resonant cavity after abrupt turn on of the incident beam. If the reflectivity of the input mirror is less than the impedance matching value the reflected light evolves as shown in the left hand diagrams; if the reflectivity is equal to the impedance matching value, the reflected power decays to zero and the phase may or may not reverse; if the reflectivity is greater than the impedance matching value the reflected light decays but never reaches zero.

indicates of how to change the cavity to move in the direction of impedance matching. The transient behavior of E^{ref} after an abrupt turn on of the incident field E^{inc} provides such a clue. It indicates whether the reflectivity of the input mirror is too high or too low for impedance matching, and gives an indication of how much adjustment is necessary. This transient behavior is shown in Fig. 9.4, and it is readily observed in numerical models. The presence of a phase reversal and amplitude rebound shown in the left panel of the figure indicates the input reflectivity is too low to impedance match. The asymptotic approach to a nonzero reflection without phase reversal or amplitude rebound shown in the right panel indicates the input reflectivity is too high. Impedance matching is the nearly complete disappearance of the reflected wave as shown in the center panel.

9.1.3 Internally generated waves

For waves that are generated entirely inside the cavity, ($S^{inc} = 0$), and the following relations apply:

$$S^{in} = S^{out} R^{out} R^{in}, \tag{9.26}$$

$$\Delta S = S^{out} - S^{in} = S^{in} \frac{(1 - R^{out} R^{in})}{R^{in} R^{out}}, \tag{9.27}$$

$$S^{in} = \Delta S \frac{R^{in} R^{out}}{1 - R^{in} R^{out}}, \tag{9.28}$$

$$S^{out} = \Delta S \frac{1}{1 - R^{in} R^{out}}, \tag{9.29}$$

$$S^{em} = \Delta S \frac{1 - R^{out}}{1 - R^{out} R^{in}}. \tag{9.30}$$

The emission efficiency is

$$\frac{S^{em}}{\Delta S} = \frac{1 - R^{out}}{1 - R^{out} R^{in}} \leq 1. \tag{9.31}$$

9.1.4 Cavity loss

We include parasitic cavity losses in our analyses by assigning an output transmission V to one of the mirrors to represent the parasitic round trip cavity loss. For impedance matched waves V will be added to the true mirror transmission of the output (right hand) mirror of the ring cavity. Including it in the right mirror rather than the left is preferred because it allows us to more easily search for the impedance matching reflectivity. The output transmission is then set to ($T^{out} = T^{true} + V$). The true output power is the total output power corrected by the factor (T^{true}/T^{out}). For internally generated waves the cavity loss will be added to the left mirror transmission in the same way.

9.1.5 Constant field approximation

Cavity mixing analysis always invokes a solution of the nonlinear mixing equations appropriate to the conditions in the cavity. Our standard assumption is that all resonated waves are strongly resonated, meaning the losses per round trip due to output coupling plus parasitic losses are small. This means the strength of the resonated wave is nearly constant throughout the length of the cavity and over the length of the crystal. We will use S^{in} as the strength of a resonated wave over the full length of the crystal. This approximation is often called the mean field approximation. We could just

a well use S^{out} or $([S^{in} + S^{out}]/2)$, but we arbitrarily chose S^{in} for the sake of simplicity and consistency. Of course, in practice a resonated wave is not always strongly resonated, and in such cases a numerical model can be used to give precise solutions. However, even in those cases the analysis we present should give insight into the principles involved in optimizing the device, as well as offering a good initial set of cavity parameters.

In this chapter we will analyze only mixing processes that do not include birefringent walk off of any beam. This is the usual circumstance for practical CW cavity devices, for example when using periodically poled crystals, or when using uniaxial or biaxial crystals that are phase matched along a directions without walk off. We also assume the three beams are collinear and spatially overlapped.

9.1.6 Gaussian beams

Our theoretical analysis of intracavity mixing throughout this chapter is based on plane waves. Diffractive treatments of various devices are available in the literature[122, 205, 206, 207, 163, 208]. However, our approach is to keep the analysis as simple as possible by using plane waves. We will derive numerous plane-wave expressions for CW cavity devices based on irradiances scaled to $S_\circ$. In many cases the resulting expressions can be simply and accurately adapted to Gaussian beams by replacing the irradiances scaled to $S_\circ$ with powers scaled to $\mathcal{P}_\circ$. This procedure was discussed in Secs. 7.4.4-7.4.6. In place of the plane-wave irradiance solution for weak sum frequency mixing,

$$S_3 = \frac{\omega_3^2}{\omega_1 \omega_2} \frac{S_1 S_2}{S_\circ} \tag{9.32}$$

we use the Gaussian beam power relation

$$\mathcal{P}_3 = \frac{\omega_3^2}{\omega_1 \omega_2} \frac{\mathcal{P}_1 \mathcal{P}_2}{\mathcal{P}_\circ}. \tag{9.33}$$

Similarly, in place of the weak difference frequency mixing solution,

$$S_2 = \frac{\omega_2}{\omega_1} \frac{S_3 S_1}{S_\circ} \tag{9.34}$$

we substitute the Gaussian beam power version

$$\mathcal{P}_2 = \frac{\omega_2}{\omega_1} \frac{\mathcal{P}_3 \mathcal{P}_1}{\mathcal{P}_\circ}. \tag{9.35}$$

These expressions serve to define $\mathcal{P}_\circ$. Its value is easily found by substituting into these equations the three powers found by numerically modeling Gaussian beam interactions under weak mixing conditions with the focusing conditions appropriate for the cavity device.

This translation of the plane-waves analysis to Gaussian beams by substitutions ($S_i/S_\circ \rightarrow \mathcal{P}_i/\mathcal{P}_\circ$) works well if none of the beams is strongly depleted in a single pass of the crystal, and if the ideal focusing conditions of Boyd and Kleinman are used. If these conditions are not met, small adjustments to the input powers or the phase matching conditions may be necessary to match Gaussian beam performance to the plane-wave predictions (see Secs. 7.4.4-7.4.6). We provide several examples in the Exercises at the end of this chapter.

9.2 Cavity sum frequency mixing

A cavity sum frequency mixer can resonate any combination of the three waves so there are five types of sum mixers (the two red waves are considered equivalent). Resonating the blue wave can enhance mixing efficiency just as resonating one or both of the red waves can. However, usually the red waves are resonated because this tends to reduce photo refractive damage which is more likely with strong blue light. It also tends to reduce heating due to linear absorption which is often greatest for the blue wave. It is also easier to align the cavity to resonate the relatively strong red beams than the initially very weak blue beam. In this section we analyze each of the five sum frequency designs, and describe conditions that must be met to achieve maximum conversion for each. We also discuss how to use numerical models to maximize mixing efficiency in any situation, including those where analytic expressions are too difficult to bother with.

9.2.1 Sum: Wave one resonated

This design is particularly useful if wave two has a broad spectrum so it cannot be resonated in the cavity, or if wave two must be tuned and you don't welcome the challenge of keeping the cavity resonant with more than one wave.

Lossless mixing

Ideal lossless mixing, diagrammed in Fig. 9.5, would achieve perfect conversion of both red waves to the blue. This implies equality of the photon fluxes of the two incident red waves, as well as impedance matching wave one to the active cavity so there is no light wasted in reflection from the input mirror. Assuming the cavity resonance is strong, resonant wave one will be much stronger inside the cavity than nonresonant wave two. The solution to the plane-wave mixing equations given by Eqs. (3.105)-(3.107) for strong wave one, with ($\Delta k = 0$) and ($S_3^{in} = 0$), expressed in terms of

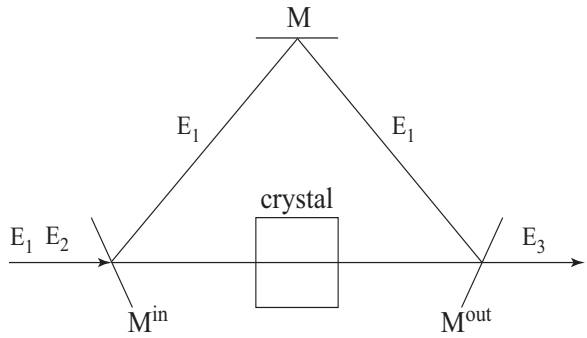

FIGURE 9.5. Diagram of an ideal singly resonant sum frequency mixer. Fields one and two are incident from the left, field one circulates in the cavity, and field three is emitted to the right. The other possible fields are all zero.

irradiances entering and exiting the crystal, is

$$S_2^{out} = S_2^{in} \cos^2 \gamma L, \tag{9.36}$$

$$S_3^{out} = S_2^{in} \frac{\omega_3}{\omega_2} \sin^2 \gamma L, \tag{9.37}$$

where

$$\gamma L = \sqrt{\frac{\omega_3}{\omega_1} \frac{S_1^{in}}{S_\circ}}, \tag{9.38}$$

with $S_\circ$ defined in Eq. (9.1). Complete conversion of wave two requires S_1^{in} to be set to make $(\gamma L = \pi/2)$, or

$$S_1^{in} = \frac{\pi^2}{4} \frac{\omega_1}{\omega_3} S_\circ. \tag{9.39}$$

Assuming S_1^{inc} is less than this, cavity enhancement is used to raise its circulating irradiance to this value. Complete conversion of wave two in a lossless crystal also implies by energy conservation

$$\Delta S_1 = -\frac{\omega_1}{\omega_2} S_2^{inc}. \tag{9.40}$$

The second requirement for ideal mixing is impedance matching wave one to the cavity. From Eq. (9.22) with $(R^{out} = 1)$, this requires

$$\Delta S_1 = -S_1^{inc}, \tag{9.41}$$

which, combined with Eq. (9.40), imposes photon balance between waves one and two incident on the cavity. Further, according to Eq. (9.14), an

impedance match requires

$$T_1^{in} = \frac{S_1^{inc}}{S_1^{in}}. \tag{9.42}$$

Using Eq. (9.39) plus ($S_1^{inc} = [\omega_1/\omega_3]S_3^{em}$) gives the impedance matching transmission

$$T_1^{in} = \frac{4}{\pi^2}\frac{S_3^{em}}{S_\circ} = \frac{4}{\pi^2}\frac{S_1^{inc} + S_2^{inc}}{S_\circ}. \tag{9.43}$$

This expression will reappear later as the relation between the pump irradiance and the output coupler transmission for an ideal, singly resonant parametric oscillator. This is not surprising since the ideal singly resonant sum mixer is a time reversed replica of the ideal singly resonant OPO.

Efficiency in a lossy cavity

Parasitic cavity loss can be simulated by setting ($R_1^{out} = 1 - V_1$) where V_1 is the fractional parasitic loss per cavity round trip. The dual goals are still to impedance match wave one and to completely deplete wave two. The photon flux of the incident wave one must exceed that of wave two because part of wave one will be wasted by the parasitic cavity loss. We wish to find the input mirror reflectivity R_1^{in} and the input irradiance for wave one S_1^{inc} that accomplish these dual goals. Complete conversion of wave two again implies

$$\Delta S_1 = -\frac{\omega_1}{\omega_2}S_2^{inc} \tag{9.44}$$

and

$$S_1^{in} = \frac{\pi^2}{4}\frac{\omega_1}{\omega_3}S_\circ. \tag{9.45}$$

Impedance matching requires

$$S_1^{inc} = T_1^{in}S_1^{in}, \tag{9.46}$$

which, according to Eq. (9.22), can be expressed

$$\Delta S_1 = S_1^{inc}\frac{R_1^{in} - R_1^{out}}{T_1^{in}R_1^{out}}. \tag{9.47}$$

These four relations can be solved to give

$$S_1^{inc} = \left(\frac{\pi^2}{4}\frac{\omega_1}{\omega_3}S_\circ - \frac{\omega_1}{\omega_2}S_2^{inc}\right)V_1 + \frac{\omega_1}{\omega_2}S_2^{inc}, \tag{9.48}$$

$$R_1^{in} = (1 - V_1)\left(1 - \frac{4}{\pi^2}\frac{\omega_3}{\omega_2}\frac{S_2^{inc}}{S_\circ}\right). \tag{9.49}$$

The V_1 term on the right side of Eq. (9.48) is the irradiance required to overcome the parasitic cavity loss, while the second term is the irradiance

required to balance the photons in wave two. Any wave one irradiance in excess of that specified by Eq. (9.48) is not useful and actually leads to reduced conversion efficiency. Excess wave one irradiance can be accommodated by increasing V_1. This would make it easier to resonate the wave since the cavity finesse would be reduced.

If the irradiance available in wave one is less than specified by Eq. (9.48), the conversion efficiency of both waves one and two will suffer. The question then is how to maximize the conversion with the available laser power. In other words, what is the best choice for R_1^{in} given the available S_1^{inc}? It is still desirable to impedance match the cavity because that maximizes S_1^{in}, even though wave two cannot be completely converted. According to Eq. (9.22) impedance matching wave one implies

$$\Delta S_1 = S_1^{inc} \frac{R_1^{in} - R_1^{out}}{T_1^{in} R_1^{out}}, \tag{9.50}$$

and the solution to the mixing equations given by Eq. (9.36), assuming $(S_2^{inc} = S_2^{in})$, is

$$\Delta S_2 = -S_2^{inc} \sin^2 \gamma L. \tag{9.51}$$

Equating the photon losses of waves one and two in passing through the crystal gives

$$S_1^{inc} \frac{R_1^{in} - R_1^{out}}{T_1^{in} R_1^{out}} = -\frac{\omega_1}{\omega_2} S_2^{inc} \sin^2 \gamma L. \tag{9.52}$$

Equation (9.52) is transcendental so R_1^{in} must be found using numerical techniques. However, if the conversion is small enough that $(\gamma L \ll 1)$ we can approximate $(\sin^2 \gamma L)$ as $(\gamma^2 L^2)$ and Eq. (9.52) can be solved to find the impedance matching reflectivity

$$R_1^{in} = \big(1 - V_1\big)\left(1 - \frac{\omega_3}{\omega_2} \frac{S_2^{inc}}{S_\circ}\right). \tag{9.53}$$

For intermediate gains where this approximation for $(\sin \gamma L)$ is inaccurate, it is quite easy to adjust R_1^{in} to its impedance matching value using numerical models of the device. The value of R_1^{in} can be varied until the reflected wave S_1^{ref} disappears.

Exercise 6 illustrates sum frequency mixing with wave one resonant, modeled with the plane-wave model PW-cav-LP.

Stability

We pointed out in earlier chapters that single-pass sum frequency mixing that approaches 100% conversion efficiency is unstable against slight upsets to the mixing conditions. Small changes in the photon balance of the red

Index